Vapor Phase Intercalation of Cesium into Black Phosphorous

Usman O. Abu, Md Rajib Khan Musa, Manthila Rajapakse, Bhupendra Karki, Dinushika Vithanage, Ming Yu, Gamini Sumanasekera, Jacek B. Jasinski**

Authors /Affiliations

Usman O. Abu, Jacek Jasinski

Conn Center for Renewable Energy Research, University of Louisville

Louisville, KY, 40292, United States

Md Rajib Khan Musa, Manthila Rajapakse, Bhupendra Karki, Dinushika Vithanage, Ming Yu, Gamini Sumanasekera

Department of Physics and Astronomy, University of Louisville

Louisville, KY, 40292, United States

*Corresponding authors: jacek.jasinski@louisville.edu, gamini.sumanasekera@louisville.edu

Abstract

Cesium vapors were charged into black phosphorous (BP) flakes at varied times and at a temperature gradient of 150^{o}C. The x-ray diffraction (XRD) measurements of these samples suggest a reduction in the strength of the van der Waal interactions between BP layers leading to the loss of coherence of out-of-plane peaks. At the same time, the three main Raman modes of BP (A_g^1, B_{2g}, and A_g^2) steadily redshifted as exposure times were increased, with modes B_{2g} and A_g^2 shifting faster than A_g^1. After initial rapid downshifts of active BP phonon modes, this intercalation strategy showed its limits following prolonged exposure times. Saturation of BP flakes by Cs vapors ensued and the kinetics was fitted with an exponential decay function. Furthermore, the thermoelectric power (TEP) of cesiated BP exhibited an inversion in sign from positive to negative around 400 K, lending credence to the transformation of as-prepared BP which is a p-type semiconductor to an n-type equivalent due to Cs atom intercalation driven shifting of the Fermi level toward the conduction band of BP and the donation of electrons from Cs. Density functional theory (DFT) calculations were used to delve deeper into understanding Cs intercalation on the structural evolution of BP.

1. Introduction

Black phosphorous (BP) has recently attracted the interest of researchers the world over because of its impressive properties; viz, band gap with wide range for tuning, elevated carrier mobility, a distinctive layer structure, and strong anisotropy of its structure and properties [1, 2]. Bulk BP was first synthesized over a century ago at extreme temperatures and pressures using white phosphorous precursors [3]. Following the successful exfoliation of graphene from graphite by Geim and Noveselov in 2004 [4], two dimensional (2D) materials became a subject of intense interest. Phosphorene, a 2D product of BP, was first exfoliated in 2014 [5]. Owing to sp^3 hybridization of its atoms, phosphorene possess a puckered honeycomb structure; a deviation from the plain atomic sheets which characterize graphene and a host of other 2D materials [6, 7]. Phosphorene has a tunable direct bandgap of approximately 0.3 – 2.0 eV, a p-type charge carrier mobility of about 6000 $cm^2 V^{-1} s^{-1}$ and unique anisotropic properties [6-8]. With these excellent catalog of features, phosphorene has found lots of applications in: energy storage[2, 9], catalysis[5, 10], optoelectronics[11] , field effect transistors[5, 12], etc.

Identical with other 2D Van der Waal (vdW) materials, foreign atoms can be introduced into the galleries of BP through intercalation which mostly results in the tuning of bandgaps and phase transitions [7, 9]. Intercalation have been accomplished by different driving forces: electrochemical[7], pressure [6], thermal [13] etc. There have been spirited efforts to obtain black phosphorous intercalation compounds (BPICs) using lithium, sodium, cesium, rubidium, iodine, ammonia and pyridine [13, 14]. Maruyama et al. studied the electronic properties BP single crystals, synthesized by growth in melted bismuth, intercalated with Li, Cs, and I. Here, Cs was intercalated into BP by homogenously heating them in a small tube [15]. They observed that the resulting compound exhibited a metallic character, where resistance increased linearly with temperature. Zhang et al.

intercalated black phosphorous with diverse metals (Li, K, Rb, Cs, and Ca) dispersed in ammonia [14]. They reported the disappearance of X-ray diffraction (XRD) peaks associated with pristine BP save for (020), (040) and (060) upon intercalation. The resulting black phosphorous intercalation compounds (BPICs) displayed superconducting properties at a transition temperature (T_c) of 3.8 K. Abellan et al. synthesized BPICs by reacting BP with different alkalis [13]. They gained insights into what is to be a novel family of intercalation compounds. However, there have not been any attempt to give a fundamental understanding of the mechanism of intercalation of BP in terms of structural and spectroscopic information by subjecting it to pristine vapors of cesium at varied times and measuring thermoelectric power (TEP) of BP as it is being intercalated by Cs vapors.

Herein, we report insights on the structural evolution of BP as it is intercalated with Cs vapors in a two-zone thermal assisted vapor-phase intercalation and the effects of Cs vapors on the TEP of BP. Structural evolution of intercalated BP was investigated using XRD and Raman spectroscopy, the energy dispersive x-ray spectroscopy (EDX) in scanning electron microscope (SEM) was used to determine the extent of intercalation and elemental composition at different times and the x-ray photoelectron spectroscopy (XPS) was used to measure the binding energy of intercalated samples and estimate elemental composition. The results gotten from the structural evolution measurements were further explained using density functional theory (DFT) calculations.

2.0 Methods

2.1. Synthesis of Black Phosphorous

Crystals of BP were synthesized using the short transport growth method[16]. Red phosphorous (500 mg), tin (25 mg) and tin iodide (15 mg) were loaded into a quartz ampoule. The ampoule was then sealed at a vacuum of 10^{-6} Torr and annealed in a furnace at 615^{o}C while a temperature gradient of 50^{o}C was maintained between the extremes of the tube. Further details on this synthesis can be sourced from previous works[6, 16].

2.2. Thermally Assisted Vapor Phase Cs Intercalation

Cs was supplied by Chemetall Gmbh, Frankfurt, Germany. The loading of Cs and BP in an ampoule was done in a nitrogen filled glovebox (< 20 ppm O_2, H_2O) to maintain an inert environment. Cs was placed in a 3" sized beaker and placed at opposite ends of a pyrex ampoule with BP in a molar ratio of 1:2.5 [17]. The loaded ampoule was covered airtight with paraffin and sealed at a vacuum of 10^{-5} Torr (Figure 6). The sealed ampoule was carefully placed in a furnace where the cesium end was placed at the hot side and annealed at 360^{o}C for 5 hours at a temperature gradient of 150^{o}C. Additional samples were prepared and annealed at same temperature for 10, 20 and 35 hours. A thin film of Cs was deposited on the walls of the ampoule signifying not all the cesium was intercalated into the BP. Upon cooling the sealed ampoule was opened in a nitrogen filled glovebox to prevent deintercalation of cesium. Part of the intercalated BP was taken out and placed on a glass-slide which was then covered with an adhesive Kapton tape and sealed completely around edges to prevent oxidation. The Kapton-covered sample was used for Raman and X-ray diffraction measurements.

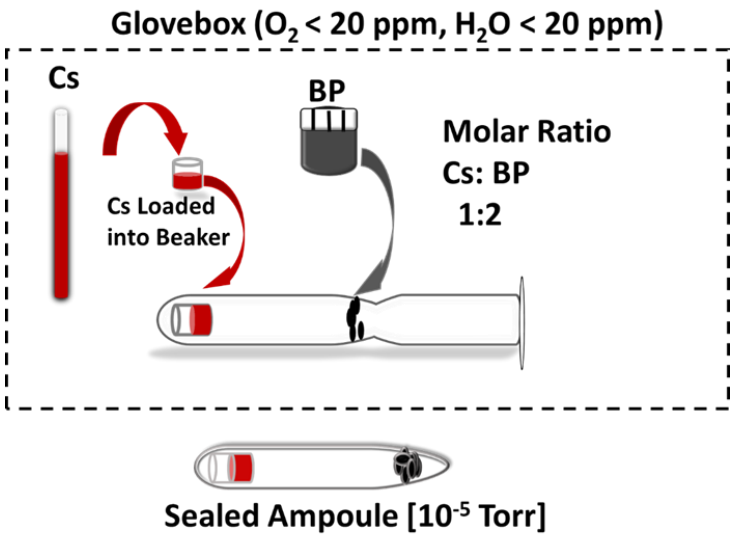

Figure 1. A schematic of the loading process of the zones in a Pyrex ampoule sealed at 10^{-5} Torr. The section enclosed in a dotted box was carried out in the glovebox while the unenclosed part was done in ambient conditions.

2.3. Characterization

Raman measurements were done using Renishaw inVia™ with 632 nm He – Ne laser, after calibration with Si wafer at 520 cm^{-1}. XRD patterns of pristine and Cs-intercalated BP samples were measured using Bruker™ Discovery D8 XRD system. SEM imaging, EDX analysis, and elemental mapping was performed using Tescan Vega 3 electron microscope equipped with an EDAX EDX detector[18]. A few selected highly-cesiated samples were also analyzed using transmission electron microscopy (TEM) in a 200 kV filed emission gun Tecnai F20 (FEI, Inc.) microscope. This included elemental mapping of individual BP-Cs flakes performed using a nanoprobe and the attached TEAM EDX system (EDAX, Inc.). XPS spectra of selected BP-Cs samples were executed with a VG Scientific MultiLab 3000 system, equipped with a dual-anode (Mg/Al) x-ray gun and a CLAM4 hemispherical electron energy analyzer. The measurements were performed at the base pressure in the upper 10^{-9} Torr range and a non-monochromatized Al Kα x-ray beam (hv = 1486.6 eV) was used as the x-ray source.

2.4 Thermoelectric Power Measurement

The in-situ thermoelectric power (TEP) of cesiated BP was measured by aligning two small thermocouples (Chromel (KP)/ Alumel) on a 4 mm by 4 mm^2 BP sample with the aid of little silver epoxy. An edge of the sample was mounted on an aluminum plate with a resistive heater (~ 100 Ω) underneath. The TEP of pristine BP was measured to serve as a reference to that of Cs intercalated BP which was measured subsequently. Cs was loaded in a mini-beaker in a glovebox with moisture and oxygen levels < 20 ppm respectively. The sample holder bearing the electrical leads was placed in a quartz reactor (without Cs first and later with Cs) was evacuated with a turbomolecular pump up to 10^{-7} Torr. TEP was measured carefully as the sample was heated slowly from room temperature up to 640 K within 5300 s. For TEP measurement, a temperature gradient (ΔT) was created by supplying a voltage pulse to the heater. TEP was then obtained from the slope of applied voltage (ΔV) and temperature gradient (ΔT) due to heat pulse at a given temperature [18, 19].

2.5. Computational Methods

In this study we adopted the density functional theory [20, 21] based computational calculation using VASP package [22]. The electron-ion interaction represented by Projector Augmented Wave (PAW) [23] and electron exchange-correlation interaction represented by generalized gradient approximation (GGA) [24] in the scheme of Perdew Burke Ernzerhof (PBE) [25]. For the study of Cs intercalation in the black phosphorus, a $1 \times 1 \times 2$ orthorhombic cell of black phosphorous with 16 P atoms was chosen and Cs atoms were intercalated up to 25% of concentration. The intercalated Cs atoms were distributed at the most energetically stable adsorption sites at the black phosphorus (for detail information about the distribution of intercalants in black phosphorus see Ref.[26]). The energy cutoff was set at 350 eV, and criteria for energy and force convergence were

set to be 10^{-5}eV and 10^{-4} eV/Å^{-1}, respectively. The Brillouin zone was sampled by $9 \times 9 \times 9$ *k*-point meshes generated in accordance with the Monkhorst–Pack scheme[27] in the calculations. The systems were fully relaxed using the Conjugate-Gradient algorithm[28] implemented in VASP. The local strain introduced by the Cs intercalation was fully released by allowing the free changes in the degrees-of-freedom on atomic positions, the unit cell shape, and the cell volume (*e.g.*, no restrictions on the atoms, the symmetry, and the volume) during the full relaxation process. The effect of vdW (van der Waals) interactions were considered by employing the semi-empirical correction scheme of Grimme[29, 30], implemented in the VASP package (referred as DFT-D3 in VASP code). Raman active modes were calculated using the derivative of macroscopic polarizability with respect to normal modes coordinates[31].

3.0 Results and Discussion

3.1. SEM and EDX Analysis

BP flakes get progressively inundated with Cs vapors as exposure times increased. The BP SEM image at 5 hours of exposure is shown in Figure 2a (i) while the SEM image equivalents for 10, 20 and 35 hours are shown in Figure 2b(i) – d(i) respectively. BP EDX maps are presented in Figure 2a(ii)-d(ii). Cs EDX maps are shown in Figures 2a(iii)-d(iii). There is a spread of Cs across the surface of BP as intercalation times increases. The Cs concentration for each intercalation time was calculated as the mean of EDX mappings of 25 spots around each sample. They are presented in the histograms in Figure 2a(iv)-d(iv) for successive exposure times. Cs concentrations were calculated with and without the edges of the BP flakes scanned. The latter showed higher

concentrations than the former as presented in Table S1 of the supporting information. The precursor concentration was constant for the exposure times at a ratio of 1: 2.5 (Cs: BP).

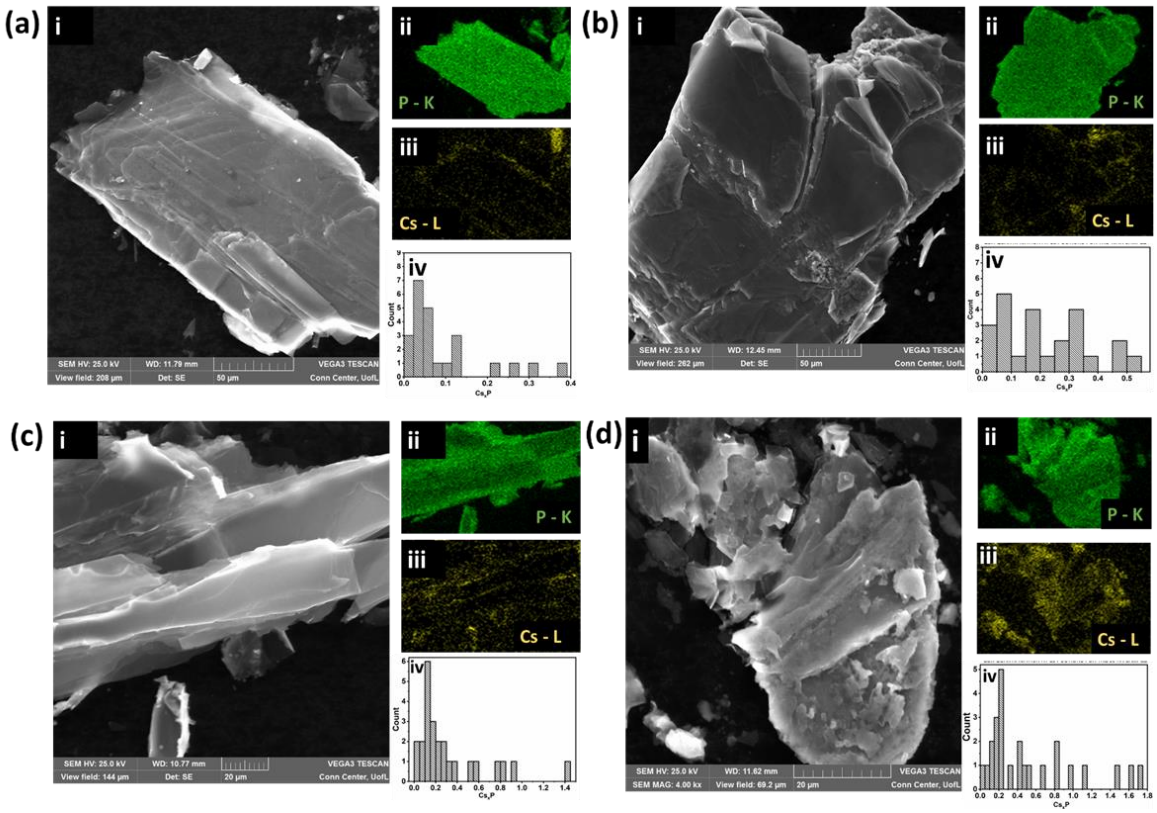

Figure 2. Morphology and elemental analysis of samples after 5 (a), 10 (b), 20 (c) and 35 (d) hours of exposure respectively. (i) SEM images showing morphology of Cs – intercalated BP flakes, (ii) EDX-based elemental P maps of these same flakes and (iii) EDX-based elemental Cs of intercalated BP flakes (iv) Cs concentration histograms based on probe analysis of 25 spots (for each sample).

3.2. Raman Spectroscopy

The Raman spectrum of BP display three vibrational modes; namely, A_g^1 (out of plane arm chair direction), B_{2g}(in − plane zigzag direction) and A_g^2 (in − plane arm chair direction). These three modes are among the six modes predicted theoretically

and the only ones allowed visible by selection rules [32]. The spectra obtained shows downshift of BP Raman modes as exposure times progressed up to 35 hours, $Cs_{0.25}$ (Figure 3a), with the A_g^1 mode shifting slower than the other two. The behavior of peak shifting was analogous to that observed for the electrochemical intercalation of BP with Li [7]. The observed downshift of the Raman modes can be understood by the fact that donor type intercalation, such as Cs-, Li-, and other alkali metal intercalation leads to an increase in the electron density of a crystal and hence, an increase in the bond lengths and decrease in the vibrational frequencies. The Raman spectra were analyzed and the peak positions as a function of exposure time were plotted as shown in Figure 3b. The data indicates that Cs-intercalation progresses relatively quickly in the first 5 hours but then starts to saturate after 35 hours of exposure to heat. This behavior is well described by an exponential decay function, $y = y_0 + Ae^{-t/\tau}$, where τ is the characteristic time constant of the process. The experimental data fitted to the exponential decay function (see Figure S1a-c for the best fits and the fitting parameters) are shown in Figure 3b. Within the experimental errors, the characteristic time constant values obtained for all three Raman modes are ~ 7 hrs. Figure 4 shows the changes in A_g^2 and B_{2g} Raman modes against the change in A_g^1 due to Cs-intercalation (green and blue circles, respectively). For both modes, the data follows the same linear trend with a slope of 1.2. The fitted linear functions and the fitting parameters are presented in Figures S2a-b. For comparison, in Figure 4, also included are the analogous sets of data for A_g^2 and B_{2g} modes against A_g^1 mode (red and black circles, respectively) obtained in our recent study on electrochemical Li-intercalation of BP (Rajapakse et al.[7]). In the case of Li-intercalation, A_g^2 and B_{2g} data also follows a linear trend, and the details of linear fitting are presented in Figures S2c-d. However, for the Li-intercalation, the slope value has significantly higher value and equals 1.6 (Figure 4). This different behavior can be attributed to the difference in size and/or mass of Cs and

Li atoms. The difference in the amount of charge transfer between these two different alkali metals and the host BP structure can also play a role. Although, more studies are needed, including theoretical modeling to fully explain this effect. In addition to different slopes of linear trends in Figure 4, there is also a difference in the amount of Raman redshifting between Cs- and Li-intercalation. As evident in Figure 3a, Cs-intercalation, even in samples subjected to a long intercalation time of 35 hours, causes relatively smaller downshift of the Raman modes than that in highly lithiated samples.

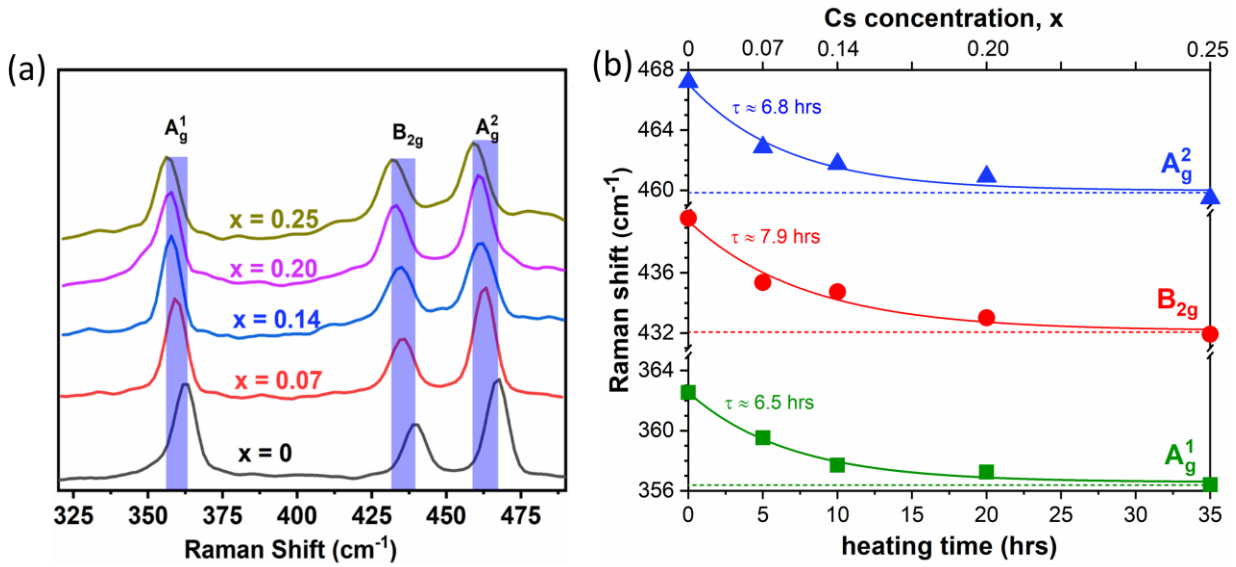

Figure 3. (a) Raman spectra of black phosphorous showing the main modes and redshifting due to Cs intercalation (b) Raman shifts of the main three BP modes as a function of exposure time (lower axis). Fitted exponential decay functions are also plotted and characteristic time constants obtained from fitting are shown. Cs concertation axis is added at the top.

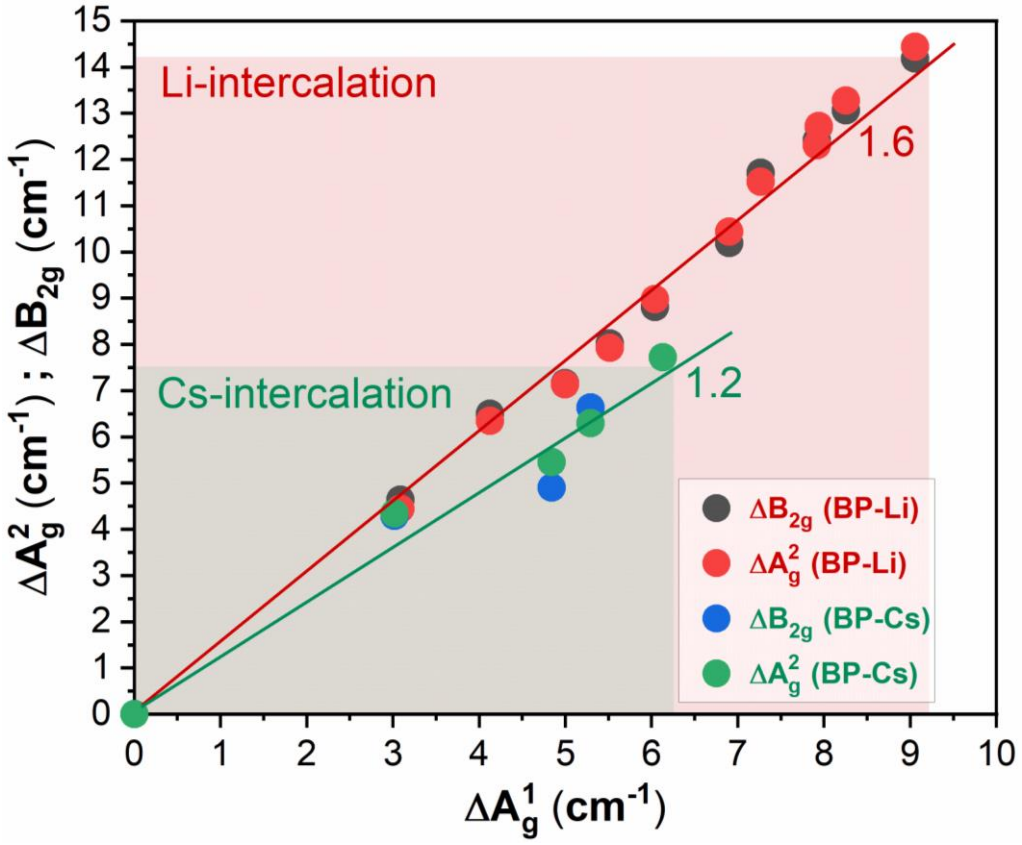

Figure 4. The changes in A_g^2 and B_{2g} Raman modes against the change in A_g^1 due to Cs- (green and blue circles) and Li-intercalation (red and black circles). The Li-intercalation data was adapted from our previous study (Rajapakse et al.[7]). In each case, A_g^2 and B_{2g} data follows the same linear trend. However, the linear coefficients obtained for Cs- and Li-intercalation are significantly different and are equal 1.2 and 1.6, respectively. Besides, Cs-intercalation causes visibly smaller redshifting of the Raman modes.

3.3. X-Ray Diffraction

The XRD patterns of BP samples cesiated at different exposure times are shown alongside the XRD pattern of pristine BP in Figure 5a. The intensity of the pattern from pristine BP was scaled down by a factor 0.12 for the ease of plotting alongside the other patterns. Most of the characteristic BP peaks vanished upon cesiation due to the loss of coherence in the out – of – plane direction that also led to much weaker peaks of (020), (040) and (060) planes [7]. In addition, there were no new

XRD peaks because of intercalation. Zhang et al. explains this occurrence as the result of the limited depth of intercalation in BP and the extended depth of x – rays into the volume of the sample during the probe [14]. The (202) peak which is related to an in – plane structure remained visible even after exposure for 35 hours, which indicates the deviation of BP from its crystalline form as Cs vapors are charged into its vdW gaps. Figures 5b and 5c respectively shows high resolution scans of (040) and (060) XRD peaks which are being split progressively as exposure times increased. Albellan et al. observed splitting as they intercalated BP with sodium and potassium [13]. This can be attributed to the gliding of those planes and formation of new phases as exposure times increased [13, 33]. The intensity of intercalated samples significantly dropped compared to pristine BP. Table S2 shows the interatomic distances of split peaks in (060).

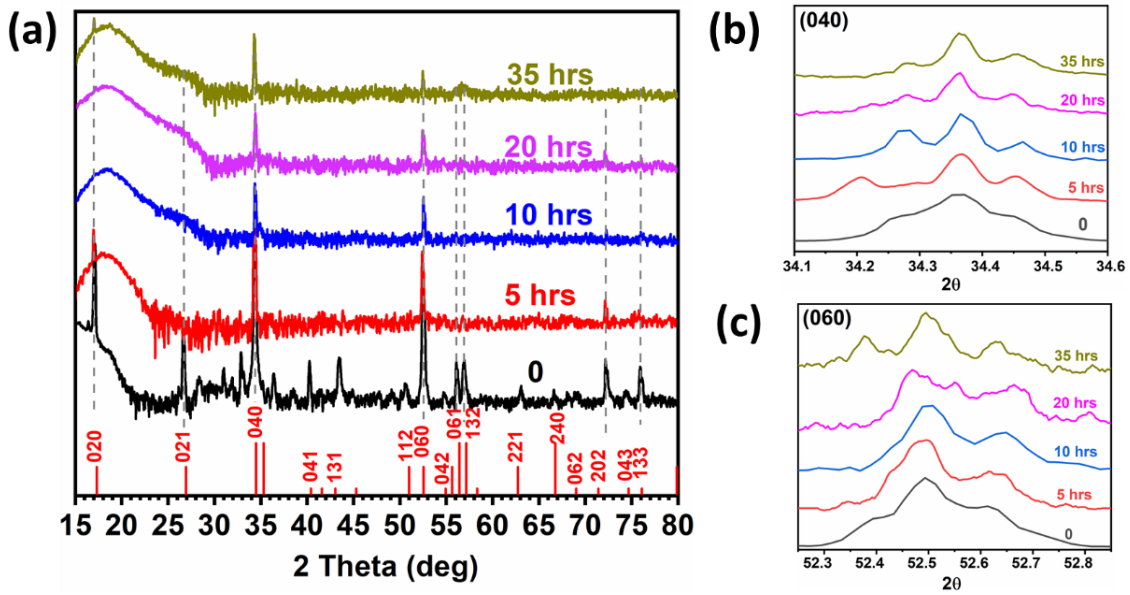

Figure 5. (a) X-ray Diffraction (XRD) spectra of the samples are stacked. The intensity of the pristine sample was reduced by a factor 0.12 for ease of plotting (b) High resolution XRD of (040) showing its evolution as time progresses (c) High resolution XRD of (060) showing its evolution as time progresses.

3.4. X-ray Photoelectron Spectroscopy

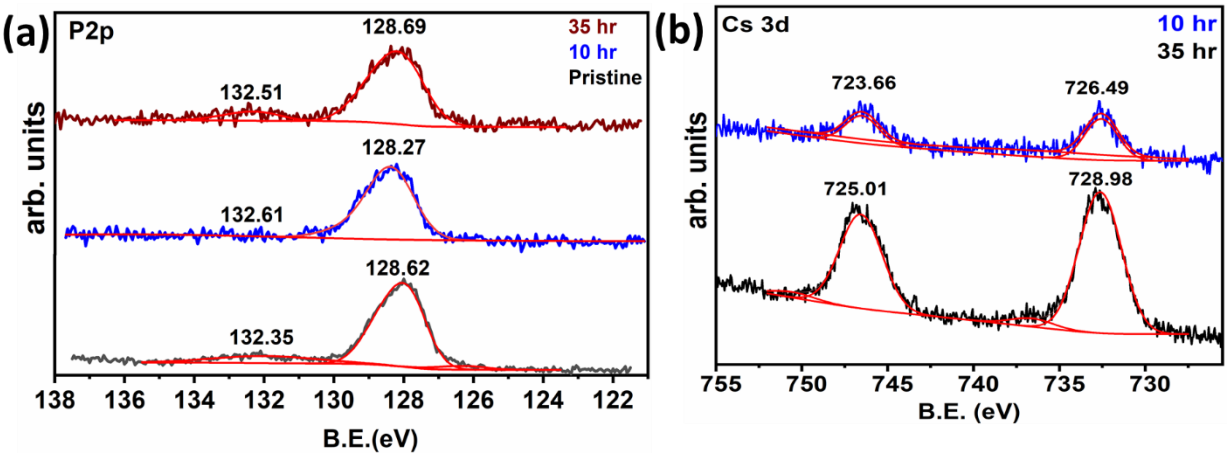

Figure 6: (a) XPS P2p spectra for pristine and Cs – Intercalated BP (b) XPS Cs 3d spectra for Cs – Intercalated BP

The XPS spectra for pristine and Cs-intercalated BP are shown in figure 6. Figure 6a shows high resolution P2p phosphorous spectra. BP peaks were visible around 128 eV and an oxidized portion with relatively smaller intensity showed peaks around 132 eV respectively; this is in agreement with Gomez-Perez et al.[34]. The absence of new peaks on the P2p spectra for intercalated BP indicates that no new phases were formed. Figure 6b shows the doublet pair structure of Cs 3d for two levels of intercalation: 10 hours and 35 hours. The intensity of the 35 hour spectrum also increased indicating more Cs composition. The calculated Cs composition based on XPS measurements are presented in table S.1.

While BP shows satisfactory stability in ambient conditions, same cannot be said about phosphorene. These constraints arise from high reactivity of phosphorene with oxygen to form phosphates [35, 36]. There have been studies on methods like encapsulation, surface functionalization, liquid-phase passivation among others[35, 37], in a bid to ensure the chemical stability of phosphorene.

Theoretical studies have shown that Cs can retard the oxidation process of phosphorene[35, 38]. In Figure 6a, we observed that the oxygen peaks on cesiated BP were comparable to initial levels as seen in pristine BP.

3.5. TEM analysis

Elemental mapping of individual BP-Cs flakes showed cesium location mainly in sub-micrometer near-edge region areas. This can be clearly seen in Figures S3a-c, where a Cs-rich BP flake and its corresponding P and Cs maps are compared, with the EDS map in Figure S3d showing the composition of Cs in BP. The observation of Cs-rich near-edge regions indicates the limited diffusivity of Cs atoms inside vdW gaps of BP and agrees with the observed saturation of Raman peak shifts, discussed earlier. These cesium-rich regions show also a strong contrast variation in TEM images due to variations in local composition and strain. In particular, a high concentration of Moiré structures is observed in these regions. Examples are shown in Figure S3 e-g. This also is reflected in superlattice reflections observed in Fast Fourier Transforms (FFTs) obtained from these areas (see examples in Figure S3-h-i). Moiré structures are formed most likely due to the intercalation-induced exfoliation of BP indicated by XRD results and small relative twists between overlapping layers. In addition to Moiré structures, apparent regions of short-range ordering (SRO) were also seen occasionally as indicated by the presence of diffuse lines observed in some FFTs and Selected Area Electron Diffraction (SAED) patterns measured from these samples (see examples in Figure S3 j-k).

3.6. Thermoelectric Power Measurement

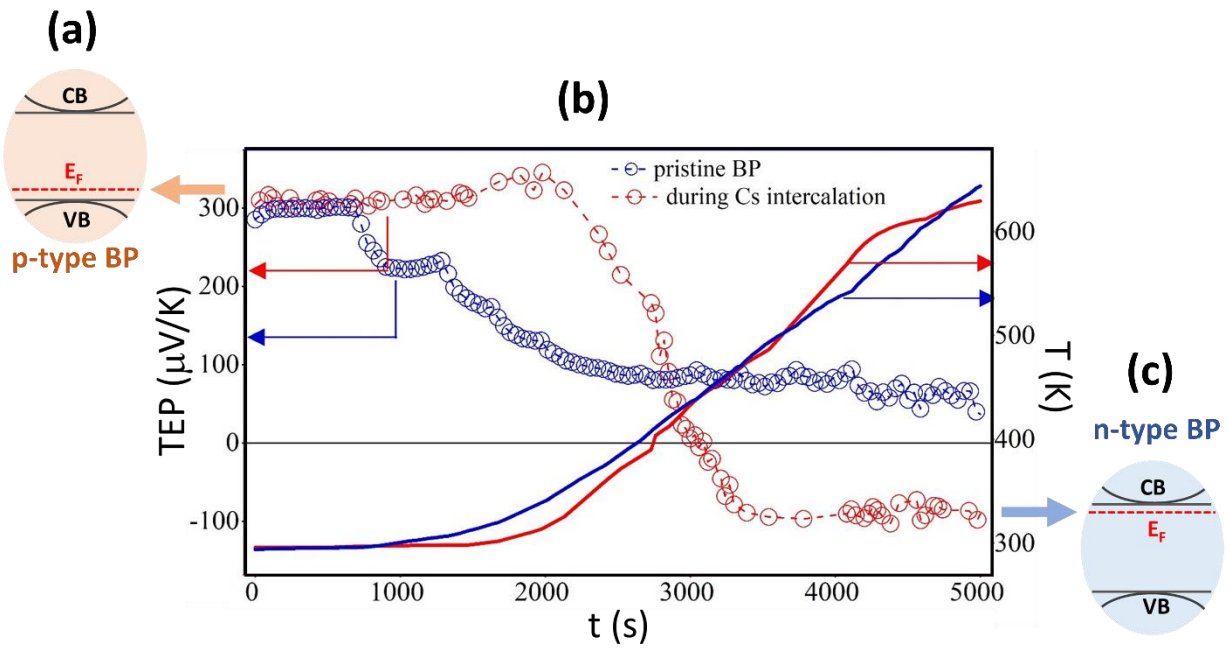

Figure 7. (a) Pristine BP as a p-type semiconductor showing positive TEP values (b) Time-dependent thermoelectric power of Pristine and Cs Intercalated BP. (c) Cs-intercalated BP as n-type semiconductor showing negative TEP values. CB and VB are conduction and valence bands, and E_F is the Fermi level.

As-prepared BP is known to be p-type (Figure 7a) presumably due to the presence of tin or other dopants introduced during growth. The TEP of pristine BP, as shown in Figure 7b decreases from around 300 μV/K to 20 μV/K systematically under heat as time evolves. This is an intrinsic behavior of BP as a semiconductor. In contrast, the TEP of BP in the presence of Cs vapor shows switching of the sign of the TEP from positive to negative ~400 K around 400 K upon cesiation further confirming intercalation. It has been established that TEP is a function of the density of states (DOS) and doping is a tool for modifying coupled electrical properties such as: electrical conductivity, TEP and thermal conductivity[39]. Upon intercalation, alkali atoms donates electrons to phosphorene resulting in the shift of its Fermi level towards the conduction band[40, 41] as shown in Figure 7c. The continuous distribution of cesium atoms changes the majority carrier of p-type BP to an n-type semiconductor as more electrons are introduced[42] making BP more metallic. Since

Cs donates most of the electrons in the outer s-orbital, it is possible that Cs atoms can form ionic bonds with P atoms thereby decreasing the band gap by pushing down the conduction band.

Cesiated BP may find applications as dispenser photocathodes in thermionic emitters, direct current electron injectors as well as injectors for polarized electrons. All these are possible due to the low work function of the materials with enhanced thermionic emission photoemission.

3.7. Structural Analysis

We have performed full structural relaxation processes for each given Cs concentration, allowing all atoms moving freely to reach their new equilibrium positions without any restriction exerted on the shape and the volume of the supercell throughout the relaxation processes so that the local strains induced by intercalated Cs atoms can be fully released. In such way, all the considered combined systems were fully relaxed and stabilized. Optimized structures of Cs_xP (x=0.0, 0.0625, 0.125, 0.1875, 0.25) and the volume of supercell as a function of the Cs concentration were depicted in Figure 8. It was found that when the Cs concentration is over 0.125, the interactions between Cs and P atoms lead to P-P bonds broken along the armchair direction and a monotonic volume expansion. Interestingly, it was found that when the intercalated Cs atoms were removed, all broken P-P bonds were reformed, and the system was relaxed back to the structures of black phosphorus with its orthorhombic symmetry (see Figure S4).

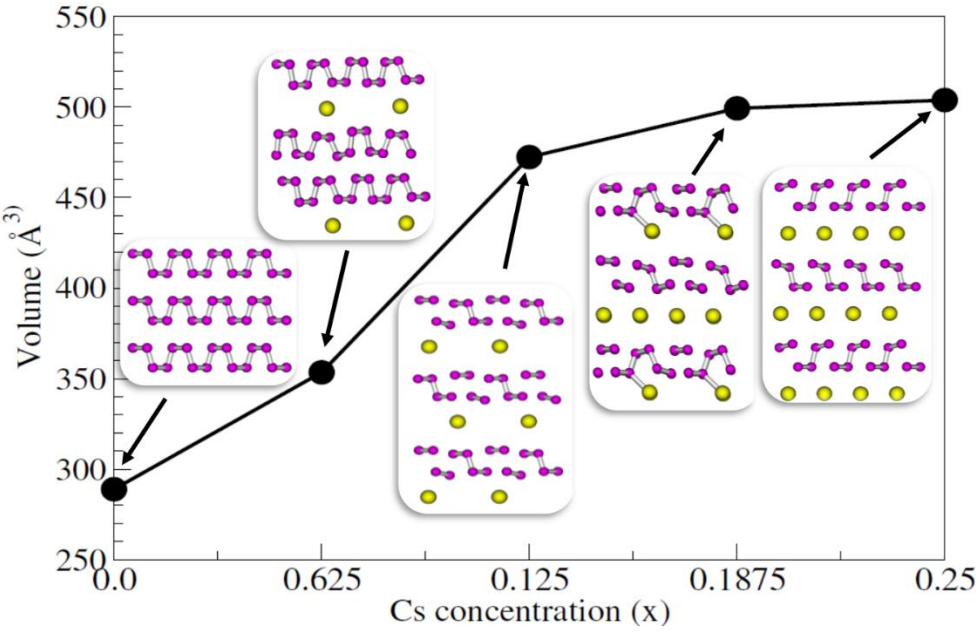

Figure 8. The volume of supercell of the Cs_xP system as a function of Cs concentration. The inserts are optimized structures of Cs_xP at x=0.0, 0.0625, 0.125, 0.1875, and 0.25, respectively. P atoms are pink colored, and Cs atoms are yellow colored.

Such phenomena can be further illustrated from local structural analyses (Figure 9). The lattice structure expands anisotropically by ~80% (see the middle panel of Figure 9a) along the out-of-plane direction (*i.e.*, along the lattice vector *b* direction indicated at the bottom of Figure 9b), as individual layers of black phosphorus are joined by weak vdW forces and Cs atoms prefer to intercalate between phosphorus layers. The in-plane lattice constants *a* and *c*, on the other hand, show a slight fluctuation (see Figure 9a) with increasing Cs concentration. A change of the lattice constant *c*, characterizing the armchair bond length, at x = 0.125 indicates the P-P bond broken along the armchair direction. While, the lattice constant *a*, characterizing the zigzag bond length, is almost unchanged, as the zigzag bonds do not break by Cs intercalation. The local distortion due to the P-P bond broken during the Cs intercalation process is also demonstrated by the change of the lattice angle of alpha (the angle between armchair and the out-of-plane, see Figure 9b and c).

Calculated Raman spectra at high frequency region and Raman shifts of the three main black phosphorus modes are shown in Figure S5. Compared with the experimental observation (Figure 3 and Figure S5), calculated results show a similar trend of a red shift in all three (A_g^1, B_{2g} and A_g^2) modes and a slightly faster downshift with Cs increasing concentration. The red shift in these modes clearly indicates that the Cs intercalation soften the P-P in-plane and out-of-plane vibration modes.

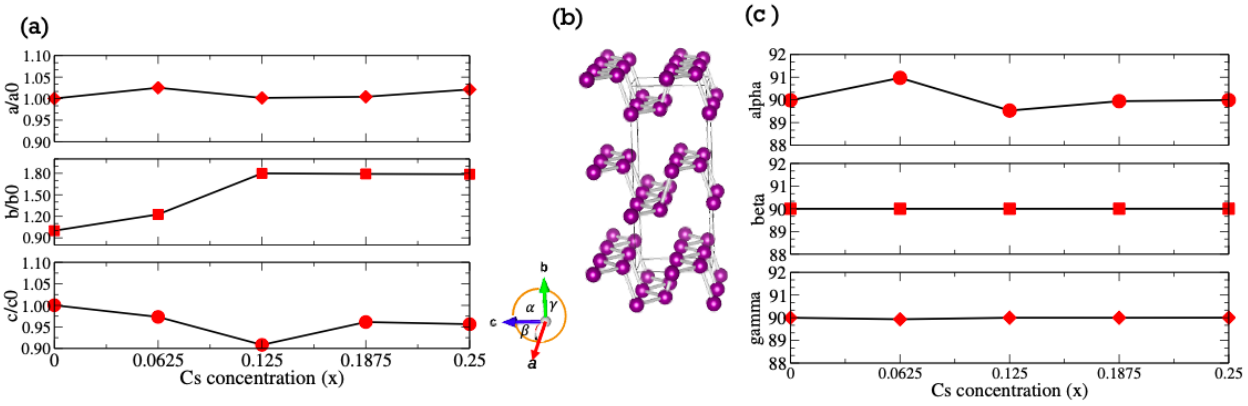

Figure 9. The Cs concentration dependence of relative lattice constants (a) and lattice angels (c) of Cs_xP system, as compared to those of pristine back phosphorus. (b) The structure of the pristine black phosphorous and its lattice vectors and angles.

We also found that the intercalation of Cs atom leads to a change in the electronic properties of the black phosphorus. The semiconductor behavior of BP transits to a metallic nature with zero band gap (Figure S6). The Fermi level was found upshifting to the conduction band, due to the charge transfer from the Cs atoms to BP, indicating the weak ionic bonding between Cs and P atoms (Figures S6 and S7). With more Cs atoms intercalated, more active charge transfers from the Cs atoms to BP and leads to the Fermi level upshifting even further, making BP more conductive.

4. Conclusion

We have driven cesium vapors into the layers of BP flakes with the aid of a temperature gradient of 150^{o}C at varied times. The XRD signatures of the heated samples confirmed the loss of coherency due to weakening of the vdW interactions between the layers of BP. We observed the weakening of out-of-plane peaks: (020), (040) and (060), while the in-plane (202) peak was not affected until 35 hours before it vanished. The high resolution XRD spectra of (040) and (060) for the different exposure times show the peak splitting which resulted from the gliding of planes.

The Raman spectroscopy revealed the systematic redshift of the Raman phonon modes of BP (A_g^1, B_{2g} and A_g^2) as intercalation times increased from 5 hours through 35 hours where B_{2g} and A_g^2 modes shifted 1.2 times faster than A_g^1 mode. The saturation kinetics of BP flakes with Cs vapors after prolonged heating showed the limits of this method of intercalation considering Cs vapors into BP layers and it tallied well with an exponential decay function. Moreover, the theoretical structural analysis of Cs intercalation into BP also exhibited similar behavior observed in the experimental Raman measurement. Raman phonon modes (A_g^1, B_{2g} and A_g^2) downshifted with increasing Cs concentrations, albeit at larger amounts relative to experimental results. This discrepancy was due to assumptions on the model of intercalation used for the calculations. Remarkably, the XPS results shows no new phases were formed at attained Cs concentration levels and the TEP evidences the p-type to n-type transformation of as-synthesized BP with a sign inversion from positive to negative at $\sim$ 400 K as cesiation proceeds under heat, evidencing the transformation of as-prepared BP from a p-type to an n-type semiconductor due to the Cs intercalation driven shift of the Fermi level toward the conduction band of BP and the donation of electrons from Cs.

Our results provide insights into the limits of intercalation of BP with Cs using the thermal-assisted vapor phase method, spectroscopic information on structure of the Cs-intercalated BP and the behavior of the TEP of BP as Cs is introduced into its layers under heat.

Acknowledgments

This work was supported by the U.S. Department of Energy, Office of Science, Basic Energy Sciences, under Award # DE-SC0019348.

Supporting Information

(a) Cesium concentration estimation. (b) Function fitting of: (i) peak position vs. exposure time in Cs vapors and (ii) changes in A_g^2 and B_{2g} Raman modes against the change in A_g^1 due to Cs- and Li-intercalation. (c) TEM characterization results. (d) Theoretical structure of $Cs_{0.25}P$ before and after relaxation (e) Theoretical Raman Spectra and peak positions of Cs-intercalated BP (f) Band Structures and Densities of State of $Cs_nP_{16.}$ (g) Tabulated d-spacing values of observed XRD (060) peak components.

References

1. Akhtar, M.; Anderson, G.; Zhao, R.; Alruqi, A.; Mroczkowska, J. E.; Sumanasekera, G.; Jasinski, J. B., Recent advances in synthesis, properties, and applications of phosphorene. *npj 2D Materials and Applications* **2017,** *1* (1), 1-13.
2. Lin, S.; Li, Y.; Qian, J.; Lau, S. P., Emerging opportunities for black phosphorus in energy applications. *Materials Today Energy* **2019,** *12*, 1-25.
3. Bridgman, P., Further Note on Black Phosphorous. *Journal of the American Chemical Society* **1916,** *38* (3), 609-612.
4. Geim, A. K.; Novoselov, K. S., The rise of graphene. In *Nanoscience and technology: a collection of reviews from nature journals*, World Scientific: **2010**; pp 11-19.
5. Li, L.; Yu, Y.; Ye, G. J.; Ge, Q.; Ou, X.; Wu, H.; Feng, D.; Chen, X. H.; Zhang, Y., Black phosphorus field-effect transistors. *Nat Nanotechnol* **2014,** *9* (5), 372-7.

6. Akhtar, M.; Zhang, C.; Rajapakse, M.; Musa, M. R. K.; Yu, M.; Sumanasekera, G.; Jasinski, J. B., Bilayer phosphorene under high pressure: in situ Raman spectroscopy. *Physical Chemistry Chemical Physics* **2019,** *21* (14), 7298-7304.
7. Rajapakse, M.; Musa, R.; Abu, U.; Karki, B.; Yu, M.; Sumanasekera, G. U.; Jasinski, J. B., Electrochemical Li Intercalation in Black Phosphorous: In-Situ and Ex-Situ Studies. *The Journal of Physical Chemistry C* **2020,** *124* (19), 10710-10718.
8. Hu, H.; Shi, Z.; Khan, K.; Cao, R.; Liang, W.; Tareen, A. K.; Zhang, Y.; Huang, W.; Guo, Z.; Luo, X.; Zhang, H., Recent advances in doping engineering of black phosphorus. *Journal of Materials Chemistry A* **2020,** *8* (11), 5421-5441.
9. Kim, S.; Cui, J.; Dravid, V. P.; He, K., Orientation-Dependent Intercalation Channels for Lithium and Sodium in Black Phosphorus. *Advanced Materials* **2019,** *31* (46), 1904623.
10. Xu, Y.; Shi, Z.; Shi, X.; Zhang, K.; Zhang, H., Recent progress in black phosphorus and black-phosphorus-analogue materials: properties, synthesis and applications. *Nanoscale* **2019,** *11* (31), 14491-14527.
11. Lei, W.; Liu, G.; Zhang, J.; Liu, M., Black phosphorus nanostructures: recent advances in hybridization, doping and functionalization. *Chemical Society Reviews* **2017,** *46* (12), 3492-3509.
12. Rajapakse, M.; Anderson, G.; Zhang, C.; Musa, R.; Walter, J.; Yu, M.; Sumanasekera, G.; Jasinski, J. B., Gas adsorption and light interaction mechanism in phosphorene-based field-effect transistors. *Physical Chemistry Chemical Physics* **2020,** *22* (10), 5949-5958.
13. Abellán, G.; Neiss, C.; Lloret, V.; Wild, S.; Chacón-Torres, J. C.; Werbach, K.; Fedi, F.; Shiozawa, H.; Görling, A.; Peterlik, H., Exploring the formation of black phosphorus intercalation compounds with alkali metals. *Angewandte Chemie International Edition* **2017,** *56* (48), 15267-15273.
14. Zhang, R.; Waters, J.; Geim, A. K.; Grigorieva, I. V., Intercalant-independent transition temperature in superconducting black phosphorus. *Nature communications* **2017,** *8* (1), 1-7.
15. Maruyama, Y.; Suzuki, S.; Osaki, T.; Yamaguchi, H.; Sakai, S.; Nagasato, K.; Shirotani, I., Electronic properties of black phosphorus single crystals and intercalation compounds. *Bulletin of the Chemical Society of Japan* **1986,** *59* (4), 1067-1071.
16. Köpf, M.; Eckstein, N.; Pfister, D.; Grotz, C.; Krüger, I.; Greiwe, M.; Hansen, T.; Kohlmann, H.; Nilges, T., Access and in situ growth of phosphorene-precursor black phosphorus. *Journal of crystal growth* **2014,** *405*, 6-10.
17. Purewal, J.; Keith, J.; Ahn, C.; Fultz, B.; Brown, C.; Tyagi, M., Adsorption and melting of hydrogen in potassium-intercalated graphite. *Physical Review B* **2009,** *79* (5), 054305.
18. Karki, B.; Rajapakse, M.; Sumanasekera, G. U.; Jasinski, J. B., Structural and Thermoelectric Properties of Black Arsenic–Phosphorus. *ACS Applied Energy Materials* **2020,** *3* (9), 8543-8551.
19. Desai, S.; Rivera, J.; Jalilian, R.; Hewaparakrama, K.; Sumanasekera, G., Studies of electronic distribution in potassium-doped mats of single-walled carbon nanotubes, double-walled carbon nanotubes, and peapods. *Journal of Applied Physics* **2008,** *104* (1), 013707.
20. Kohn, W.; Sham, L. J., Self-consistent equations including exchange and correlation effects. *Physical review* **1965,** *140* (4A), A1133.
21. Hohenberg, P.; Kohn, W., Inhomogeneous electron gas. *Physical review* **1964,** *136* (3B), B864.
22. Kresse, G.; Furthmüller, J., Efficient Iterative Schemes for Ab Initio Total-Energy Calculations Using a Plane-Wave Basis Set. *Phys. Rev. B: Condens. Matter Mater. Phys.* **1996,** *54*, 11169.
23. Blöchl, P. E., Projector augmented-wave method. *Physical Review B* **1994,** *50* (24), 17953-17979.
24. Perdew, J. P.; Chevary, J. A.; Vosko, S. H.; Jackson, K. A.; Pederson, M. R.; Singh, D. J.; Fiolhais, C., Atoms, molecules, solids, and surfaces: Applications of the generalized gradient approximation for exchange and correlation. *Physical review B* **1992,** *46* (11), 6671.
25. Perdew, J. P.; Burke, K.; Ernzerhof, M., Generalized Gradient Approximation Made Simple. *Phys. Rev. Lett.* **1996,** *77*, 3865.

26. Musa, M. R. K.; Zhang, C.; Rajapakse, M.; Jasinski, J. B.; Sumanasekera, G.; Yu, M., Li interaction-induced phase transition from black to blue phosphorene. *Physical Review Materials* **2021,** *5* (2), 024007.
27. Monkhorst, H. J.; Pack, J. D., Special points for Brillouin-zone integrations. *Physical review B* **1976,** *13* (12), 5188.
28. Gonze, X., First-principles responses of solids to atomic displacements and homogeneous electric fields: Implementation of a conjugate-gradient algorithm. *Physical Review B* **1997,** *55* (16), 10337.
29. Grimme, S., Semiempirical GGA-type density functional constructed with a long-range dispersion correction. *Journal of computational chemistry* **2006,** *27* (15), 1787-1799.
30. Grimme, S.; Antony, J.; Ehrlich, S.; Krieg, H., A consistent and accurate ab initio parametrization of density functional dispersion correction (DFT-D) for the 94 elements H-Pu. *The Journal of chemical physics* **2010,** *132* (15), 154104.
31. Porezag, D.; Pederson, M. R., Infrared intensities and Raman-scattering activities within density-functional theory. *Physical Review B* **1996,** *54* (11), 7830-7836.
32. Kang, J. S.; Ke, M.; Hu, Y., Ionic Intercalation in Two-Dimensional van der Waals Materials: In Situ Characterization and Electrochemical Control of the Anisotropic Thermal Conductivity of Black Phosphorus. *Nano Letters* **2017,** *17* (3), 1431-1438.
33. Cheng, Y.; Zhu, Y.; Han, Y.; Liu, Z.; Yang, B.; Nie, A.; Huang, W.; Shahbazian-Yassar, R.; Mashayek, F., Sodium-induced reordering of atomic stacks in black phosphorus. *Chemistry of Materials* **2017,** *29* (3), 1350-1356.
34. Gómez-Pérez, J.; Barna, B.; Tóth, I. Y.; Kónya, Z.; Kukovecz, A. k., Quantitative tracking of the oxidation of black phosphorus in the few-layer regime. *ACS omega* **2018,** *3* (10), 12482-12488.
35. Sang, D. K.; Wang, H.; Guo, Z.; Xie, N.; Zhang, H., Recent developments in stability and passivation techniques of phosphorene toward next-generation device applications. *Advanced Functional Materials* **2019,** *29* (45), 1903419.
36. Castellanos-Gomez, A.; Vicarelli, L.; Prada, E.; Island, J. O.; Narasimha-Acharya, K.; Blanter, S. I.; Groenendijk, D. J.; Buscema, M.; Steele, G. A.; Alvarez, J., Isolation and characterization of few-layer black phosphorus. *2D Materials* **2014,** *1* (2), 025001.
37. Luo, S.; Zhao, J.; Zou, J.; He, Z.; Xu, C.; Liu, F.; Huang, Y.; Dong, L.; Wang, L.; Zhang, H., Self-standing polypyrrole/black phosphorus laminated film: promising electrode for flexible supercapacitor with enhanced capacitance and cycling stability. *ACS applied materials & interfaces* **2018,** *10* (4), 3538-3548.
38. Lei, S.-Y.; Shen, H.-Y.; Sun, Y.-Y.; Wan, N.; Yu, H.; Zhang, S., Enhancing the ambient stability of few-layer black phosphorus by surface modification. *RSC advances* **2018,** *8* (26), 14676-14683.
39. Zhang, Y.; Wang, J.; Liu, Q.; Gu, S.; Sun, Z.; Chu, P. K.; Yu, X., The electrical, thermal, and thermoelectric properties of black phosphorus. *APL Materials* **2020,** *8* (12), 120903.
40. Kulish, V. V.; Malyi, O. I.; Persson, C.; Wu, P., Adsorption of metal adatoms on single-layer phosphorene. *Physical Chemistry Chemical Physics* **2015,** *17* (2), 992-1000.
41. Rajapakse, M.; Karki, B.; Abu, U. O.; Pishgar, S.; Musa, M. R. K.; Riyadh, S. S.; Yu, M.; Sumanasekera, G.; Jasinski, J. B., Intercalation as a versatile tool for fabrication, property tuning, and phase transitions in 2D materials. *npj 2D Materials and Applications* **2021,** *5* (1), 1-21.
42. Lyeo, H.-K.; Khajetoorians, A.; Shi, L.; Pipe, K. P.; Ram, R. J.; Shakouri, A.; Shih, C., Profiling the thermoelectric power of semiconductor junctions with nanometer resolution. *Science* **2004,** *303* (5659), 816-818.

For Table of Contents Only